# Intrinsic properties and mechanisms of spontaneous firing in mouse cerebellar unipolar brush cells

Marco J. Russo[1,2], Enrico Mugnaini[1,2] and Marco Martina[1]

[1]*Department of Physiology and* [2]*Department of Cellular and Molecular Biology, Feinberg School of Medicine, Northwestern University, 303 E. Chicago Avenue, Chicago, IL 60611, USA*

**Neuronal firing patterns are determined by the cell's intrinsic electrical and morphological properties and are regulated by synaptic interactions. While the properties of cerebellar neurons have generally been studied in much detail, little is known about the unipolar brush cells (UBCs), a type of glutamatergic interneuron that is enriched in the granular layer of the mammalian vestibulocerebellum and participates in the representation of head orientation in space. Here we show that UBCs can be distinguished from adjacent granule cells on the basis of differences in membrane capacitance, input resistance and response to hyperpolarizing current injection. We also show that UBCs are intrinsically firing neurons. Using action potential clamp experiments and whole-cell recordings we demonstrate that two currents contribute to this property: a persistent TTX-sensitive sodium current and a ruthenium red-sensitive, TRP-like cationic current, both of which are active during interspike intervals and have reversal potentials positive to threshold. Interestingly, although UBCs are also endowed with a large $I_h$ current, this current is not involved in their intrinsic firing, perhaps because it activates at voltages that are more hyperpolarized than those associated with autonomous activity.**

(Resubmitted 30 January 2007; accepted after revision 19 March 2007; first published online 22 March 2007)
**Corresponding author** M. Martina: Department of Physiology, Northwestern University Feinberg School of Medicine, 303 E. Chicago Avenue, Chicago, IL 60611, USA. Email: m-martina@northwestern.edu

One of the most astonishing features of neurons is their enormous range of diversity regarding shape and size of cell bodies, design and synaptic connections of dendritic and axonal cell processes, gene expression and electrical properties. These parameters cumulatively contribute to shaping the neuronal firing patterns, which constitute the final output of nearly every type of neuron. Firing patterns, although regulated by synaptic inputs, depend primarily on the cell's intrinsic properties and are often used together with the neuronal morphology and chemical markers to describe individual cell types (Freund & Buzsáki, 1996; Cauli *et al.* 1997; Parra *et al.* 1998; Molineux *et al.* 2006).

Unipolar brush cells (UBCs) are a recently established class of excitatory, glutamatergic interneurons residing in the granular layer of the mammalian cerebellar cortex (Mugnaini & Floris, 1994; Mugnaini *et al.* 1997; Nunzi *et al.* 2001). The UBC has a round or oval cell body, with diameter measuring 8–12 $\mu$m in rodents, and usually emits a single dendrite, approximately 2 $\mu$m thick and 10–30 $\mu$m long, that ends in a paintbrush-like tuft of short dendrioles within a special cerebellar glomerulus. The brush dendrioles form unusually large synaptic junctions, cumulatively measuring 20–40 $\mu m^2$ of synaptic apposition (Mugnaini *et al.* 1994; Rossi *et al.* 1995). UBCs are particularly enriched in the granular layer of the caudal cerebellar (or vestibulocerebellar) folia, which are densely innervated by primary and secondary vestibular fibres and act to integrate vestibular and visual signals into a representation of head orientation that modulates reflex behaviour (Sekerková *et al.* 2005).

Although synaptic responses and firing patterns of UBCs have been recorded both *in vitro* and *in vivo* (Rossi *et al.* 1995; Kinney *et al.* 1997; Nunzi *et al.* 2001; Billups *et al.* 2002; Simpson *et al.* 2005), the intrinsic electrical properties of these neurons remain largely unknown, in part because of the lack of readily available criteria to identify these neurons in a fresh slice and in part because of their relatively low density compared to the surrounding granule cells (Mugnaini & Floris, 1994). Synaptic stimulation of UBCs results in high frequency bursts (Rossi *et al.* 1995). Although it has been shown that these bursts occur in response to the particularly long-lasting depolarization caused by the peculiar morphology of the mossy fibre–UBC synapse (Rossi *et al.* 1995; Kinney *et al.* 1997), the contribution of intrinsic electrophysiological properties to UBCs' firing modes is not known. As said, very little is known about the

This paper has online supplemental material.

 DOI: 10.1113/jphysiol.2007.129106

intrinsic electrophysiological properties of these neurons, such as resting membrane potential, input resistance and mechanisms of firing. Also unknown is whether these neurons are capable of spontaneous firing when synaptic inputs are blocked.

In the last 20 years it has become evident that intrinsic firing is a property shared by several central neurons (reviewed by Llinás, 1988), but the molecular mechanisms underlying this phenomenon differ among cell types. Apparently, in a minority of neurons intrinsic firing depends on $I_h$, the hyperpolarization-activated current that drives pacemaking in cardiac cells (Brown & DiFrancesco, 1980; DiFrancesco, 1981). In many neuron types, either calcium currents (Bal & McCormick, 1993; Puopolo *et al.* 2005) or persistent TTX-sensitive sodium currents (Bevan & Wilson, 1999; Raman *et al.* 2000; Taddese & Bean, 2002; Do & Bean, 2003) underlie intrinsic firing.

Here we show that UBCs are intrinsically firing and that this property depends on two currents: a TTX-sensitive sodium current and a voltage-independent cationic current, which are both active during interspike intervals.

## Methods

### Slice preparation

CD1 mice, 26–38 days old, were obtained from a commercial breeder (Charles River Laboratories, Inc., Wilmington, MA; or Harlan, Indianapolis, IN, USA). Mice were deeply anaesthetized with isoflurane (0.3 ml in 1 l administered for ∼90 s) and killed by decapitation. The cerebella were quickly removed from the skull and placed in ice-cold modified artificial cerebrospinal fluid containing (mM): 87 NaCl, 25 $NaHCO_3$, 2.5 KCl, 1.25 $NaH_2PO_4$, 0.5 $CaCl_2$, 7 $MgCl_2$, 75 sucrose, 25 glucose and 1 kynurenic acid, bubbled with 95% $O_2$–5% $CO_2$. Parasagittal slices, 300 $\mu$m thick, were cut from the vermis using a vibrating blade microtome (Dosaka DTK-1000, Ted Pella Inc., Redding, CA, USA). Slices were incubated at 35°C for 20–30 min and then stored at room temperature. All recordings were performed from cells in lobules IX and X. During recording, slices were continuously superfused with physiological extracellular solution containing (mM): 125 NaCl, 25 $NaHCO_3$, 2.5 KCl, 1.25 $NaH_2PO_4$, 1.2 $CaCl_2$, 1 $MgCl_2$ and 25 glucose, bubbled with 95% $O_2$–5% $CO_2$. This solution contains 1.2 mM calcium, in accordance with the calcium concentration measured in cerebrospinal fluid (Jones & Keep, 1988; Nilsson *et al.* 1993). Slices were visualized with an Axioskop FS (Zeiss, Jena, Germany) upright microscope using infrared differential interference contrast videomicroscopy under a water-immersion 60× objective.

All experiments conformed to protocols approved by the Northwestern University Animal Care and Use Committee (ACUC). We followed guidelines issued by the National Institutes of Health and the Society for Neuroscience to minimize the number of animals used and their suffering.

### Electrophysiological recordings

Pipettes were pulled from Hilgenberg (Malsfeld, Germany) glass (1406180) using a horizontal puller (P97, Sutter, Novato, CA, USA) and filled with internal solution consisting of (mM): 140 K-gluconate, 2 $MgCl_2$, 10 EGTA, 2 $Na_2ATP$, 0.1 NaGTP, 10 Hepes, pH 7.3 with KOH. Biocytin (1 mg ml$^{-1}$) was also added to the pipette solution to allow *post hoc* visualization of the patched cells. Pipette tip resistances in working solutions ranged from 5 to 10 MΩ yielding series resistances of 15–30 MΩ.

All recordings were performed at 22–24°C using an Axopatch 200B amplifier (Axon Instruments, Union City, CA, USA). Current signals were low-pass filtered at 2 or 5 kHz (4-pole low-pass Bessel filter on amplifier) and digitized (10 kHz) using a Digidata 1321A controlled by the pCLAMP 8 software interface (Axon instruments). Signals from current-clamp recordings were sampled at 20 kHz and filtered at 10 kHz. The threshold for action potential generation was determined by calculating the first derivative of the voltage traces and by identifying for each action potential in the traces the first inflexion point in which the value of the derivative was significantly larger than the preceding baseline.

Spontaneous activity was recorded in the presence of 2 mM kynurenate and 100 $\mu$M picrotoxin to block fast synaptic transmission. Drugs and chemicals were from Sigma (St Louis, MO, USA), except ZD7288 (Tocris, Ellisville, MO, USA) and TTX (Alomone labs, Jerusalem, Israel) and were applied by bath application.

Data in the text are expressed as mean ± S.E.M. Error bars in the figures also represent S.E.M.

### Wave-clamp experiments on nucleated patches

In order to study in detail the mechanism of intrinsic firing it is necessary to accomplish the following goals: (1) record the cells' own action potentials; (2) use these recordings as voltage command under good voltage-clamp conditions; (3) have the possibility to apply the drugs reliably and with precise control of their final concentration. All these conditions are satisfied by the use of nucleated patches (Sather *et al.* 1992) from slice recordings, which allow combining nearly ideal voltage-clamp even of currents with very fast kinetics (Martina & Jonas, 1997; Baranauskas & Martina, 2006), with the identification and current-clamp recording of neurons in acute slices (Martina *et al.* 1998; Lien *et al.* 2002). Moreover, nucleated

patches maintain intact modulation pathways regulated by second messenger systems (Lien *et al.* 2002) and also allow quick exchange of the extracellular solution (Sather *et al.* 1992). Giga-seals were obtained using pipettes of ∼8 MΩ. After establishing the whole-cell configuration and recording the intrinsic firing for several seconds, negative pressure (10–15 kPa) was applied to the patch-pipette while it was slowly withdrawn. A small negative pressure (< 3 kPa) was maintained during the recordings. Nucleated patches had diameters ranging between 2.3 $\mu$m and 2.5 $\mu$m, were almost perfectly spherical and had high input resistance (≥1 GΩ). The membrane voltage trajectory recorded in whole-cell current clamp was then used as a voltage command on nucleated patches. Each individual nucleated patch was voltage clamped with the waveform previously recorded from the parent cell. All voltage values presented in this paper were corrected for liquid junction potentials (12 mV).

Drugs were applied to the patches by using a multibarrel system consisting of four glass capillaries (1.5 mm i.d.) glued together and connected to a syringe pump (WPI, Sarasota, FL, USA). The patch-pipette carrying the nucleated patch was inserted into each of the pipes, which contained Hepes-buffered ACSF (pH 7.4) plus the drugs of interest. Thus, we ensured that the solution flow was exactly the same in each barrel and no pressure artifacts were created when switching the patch from one pipe to another. The composition of the NMDG-Cl solution used to block the non-selective cationic current was the following (mM): 141 NMDG, 1.2 $CaCl_2$, 1 $MgCl_2$, 20 TEA-Cl, 3 CsCl, 20 glucose, 10 Hepes. The solution bas titrated to pH 7.3 with 142 mM HCl for a final $Cl^-$ concentration of 169 mM.

In order to optimize the compensation for capacitive transients, pipettes were always coated with Parafilm and the bath level was kept as low as possible.

### Post-hoc visualization of recorded neurons

The methods to recover the anatomy of biocytin-filled cells are similar to those described in Martina *et al.* (2000). Cells were filled with biocytin (0.5%) through the recording pipette. At the end of the recording, slices were fixed in 4% freshly depolymerized paraformaldehyde in 0.1 M phosphate buffer (PB, pH 7.4) for 24 h, at 4–6°C. After fixation slices were rinsed in PB several times and subsequently treated with hydrogen peroxide (1% in a solution made of 10% methanol, 90% PB) for 10 min and finally rinsed in PB 5 times. Slices were finally incubated in PB containing 1% avidin–biotinylated horseradish peroxidase complex (ABC, Vector laboratories, Burlingame, CA, USA) for 2 h at 20–22°C. Excess ABC was removed by several rinses in PB and the slices were developed with 0.05% 3,3′-diaminobenzidine (DAB). Finally slices were embedded in Mowiol (Aldrich, Milwaukee, WI, USA) to be examined by bright field light microscopy.

## Results

### UBCs and granule cells differ in intrinsic electrical properties

We compared the intrinsic electrical properties of UBCs and granule cells in lobules IX and X of the cerebellum in acute slices obtained from 26- to 38-day-old-mice. UBCs were tentatively distinguished from granule cells by searching for neurons with slightly larger, more ovoid cell bodies within the granular layer (Fig. 1*A* and *B*). Initially, the cell identification was confirmed *post hoc* by anatomical visualization of the biocytin filled neurons (Fig. 1*C* and *D*). Comparison of anatomically identified UBCs and granule cells led us to uncover electrophysiological properties that may distinguish between these two neuronal types. As shown in Fig. 1*E*, UBCs and granule cells responded differently to current injection. Cells were recorded in current-clamp without injection of any bias current and tested by delivering 500 ms long current pulses of amplitude ranging from −200 pA to +140 pA (in 20 pA steps). The voltage responses of the UBCs (Fig. 1*E*, upper traces) were highly reproducible from cell to cell and clearly different from those of granule neurons (Fig. 1*E*, lower traces). In particular, UBCs showed strong voltage sag and rebound firing, which were not observed in granule neurons. Figure 2 shows the ratio of the initial input resistance (measured at the peak) to the resistance at steady state (last 50 ms of the pulses) in the two cell types. The value of this ratio was 2.2 ± 0.07 in UBCs and 1.2 ± 0.06 in granule cells (Fig. 2*B*, 58 and 15 cells, respectively, $P < 0.01$) suggesting a differential expression of $I_h$ between the two cell types. UBCs were also characterized by larger membrane capacitance (Dugué *et al.* 2005) and lower input resistance compared to granule cells (Fig. 2*C* and *D*). The average capacitance of UBCs was 23 ± 1 pF ($n = 62$), whereas it was only 4.5 ± 0.4 pF for granule cells (19 cells, $P < 0.01$, Fig. 2*C*). The mean input resistance (measured using 15 or 20 ms long 5 mV pulses in voltage clamp) was 527 ± 22 MΩ for UBCs and 1057 ± 202 MΩ for granule cells (62 and 19 cells, respectively, $P < 0.01$, Fig. 2*D*). Another difference between UBCs and granule cells was the maximum firing frequency, which was 99 ± 3 Hz for the UBCs and 132 ± 3 Hz for granule cells (at 21–23°C, 12 and 7 cells, respectively, $P < 0.01$, Fig. 2*E*). Accordingly, the spike half-duration was significantly longer in UBCs than in granule cells (half-duration was 1.67 ± 0.09 and 0.74 ± 0.04 ms, respectively, 12 and 7 cells, $P < 0.01$, Fig. 2*F*).

These data show that UBCs and granule cells are characterized by different cable and firing properties, providing reliable criteria for distinguishing the two cell types.

### UBCs are intrinsically firing

Another readily observable difference between UBCs and granule cells is the fact that, in acute slices, UBCs are intrinsically firing, while granule cells are not. The intrinsic firing of UBCs is very robust: the firing frequency was almost unaffected under several different recording conditions (Fig. 3). UBCs were spontaneously firing in cell-attached recordings (Fig. 3*A*); in whole-cell configuration the frequency of firing was $11 \pm 4.7$ Hz in control conditions ($n = 8$, slices bathed in ACSF, Fig. 3*B*), and $10.2 \pm 1.4$ Hz when the synaptic activity in the slices was blocked by bath application of 2 mM kynurenic acid and 100 $\mu$M picrotoxin ($n = 41$; Fig. 3*C*). Intrinsic firing also persisted when the extracellular calcium concentration was increased from 1.2 to 2 mM (the firing frequency in the 3 neurons tested for these experiments was $4.4 \pm 0.8$ Hz in 1.2 mM calcium and $7.6 \pm 3.7$ Hz in 2 mM calcium; see the figure in the online supplemental material) or when the intracellular solution contained KCl (and no EGTA) instead of K-gluconate ($n = 5$, not shown). The robustness of the firing was further supported by the fact that intrinsic firing persisted also when ATP and GTP were omitted from the intracellular solution (in recordings where the nucleotide triphosphates were omitted the firing frequency actually increased by 37%, $n = 30$). The firing frequency of UBCs was not significantly affected even when voltage-gated calcium channels were blocked by substituting extracellular calcium with an equimolar concentration of cobalt (the firing frequency in cobalt was $91 \pm 14\%$ of control, $n = 8$, $P > 0.1$; Fig. 4*A* and *B*). Cobalt, however, induced significant changes in both the spike half-width and the amplitude of the after-hypepolarization ($175 \pm 24\%$ and $48 \pm 9\%$, $P < 0.05$ and $P < 0.01$, respectively, $n = 8$), most likely due to the blockade of calcium-activated potassium channels.

As shown in Figs 1 and 2, UBCs are characterized by their prominent voltage sag in response to hyperpolarizing current injections. However, $I_h$ blockers did not decrease the ability of these neurons to fire intrinsically; on the contrary, both ZD7288 (100 $\mu$M, Fig. 5) and caesium (3 mM, Fig. 6) unexpectedly increased the firing frequency, although the change was not statistically significant (frequency increased by $39 \pm 5\%$ in ZD7288, $n = 8$, and by $31 \pm 16\%$ in caesium, $n = 3$, $P > 0.05$ in both cases, paired $t$ test). The lack of effect of ZD7288 on the firing frequency could raise questions about the efficacy of the drug, or on the nature of the conductance underlying the 'sag' observed in response to hyperpolarizing current injection. Thus, we performed whole-cell recordings to test the effect of ZD7288. As shown in Fig. 7, the drug had the expected effects both in voltage and current clamp. In current clamp, ZD7288 completely abolished the voltage sag (Fig. 7*A* and *B*); in voltage clamp, it blocked a current with gating properties typical of $I_h$ (Fig. 7*C*). The activation curve of the ZD-sensitive current (Fig. 7*D*) shows that it had a quite negative activation range ($< -60$ mV), suggesting that the

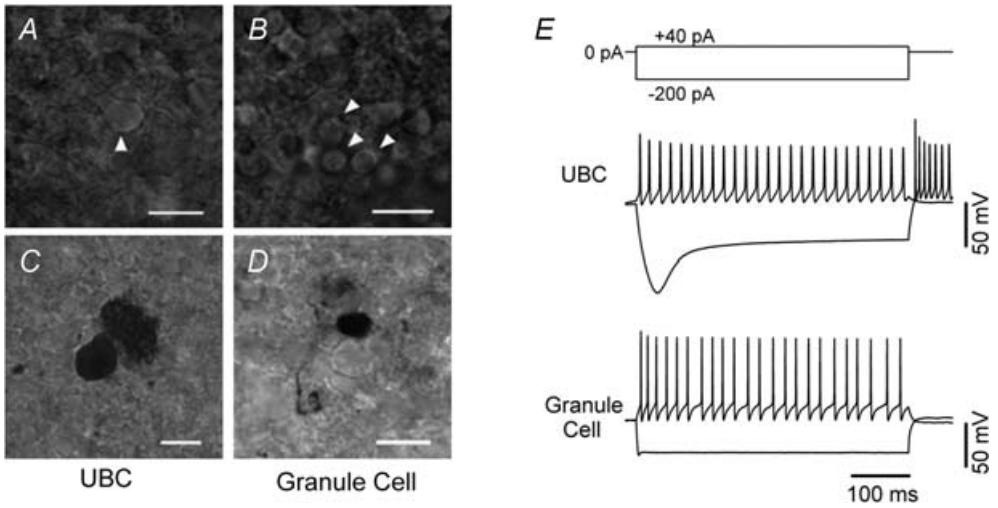


**Figure 1. Morphological and functional properties distinguish UBCs and granule cells**
*A* and B, infrared image of a UBC and granule cells (arrowheads) in an acute cerebellar slice. The UBC could be identified on the basis of larger ovoid soma and the typical brush. *C* and *D*, the identity of the cells was confirmed by biocytin staining. Calibration bars = 10 $\mu$m. *E*, current clamp recordings from a UBC and a granule cell in response to 500 ms current injections (top inset). Note the prominent difference in the responses to hyperpolarizing current injections.

lack of effect on the firing frequency is due to the fact that, during intrinsic firing, UBCs never experience membrane potentials negative enough to effectively activate $I_h$.

These data suggest that neither calcium currents nor $I_h$ play a significant role in supporting intrinsic firing of these neurons.

### Mechanisms of intrinsic firing

Since neither $I_h$ nor voltage-dependent calcium currents were essential contributors to the intrinsic firing in current-clamp recordings, we focused on the possible role of subthreshold sodium current, which has been shown to drive intrinsic firing in several neuronal types (Feigenspan *et al.* 1998; Bevan & Wilson, 1999; Raman & Bean, 1999; Raman *et al.* 2000; Taddese & Bean, 2002; Do & Bean, 2003). To test this mechanism, we designed wave-clamp experiments in which we first recorded spontaneous action potentials in whole-cell and then excised nucleated patches from the recorded neurons; these patches were used for voltage-clamp recordings in which the current-clamp recorded voltage trajectory was used as command voltage. Nucleated patches had a mean area of $\sim$18 $\mu$m$^2$ (estimated from photographs of the nucleated patches and assuming spherical shape) and an input resistance of $9.5 \pm 2.2$ G$\Omega$ ($n = 10$). The effect of TTX (300 nM) on such a recording

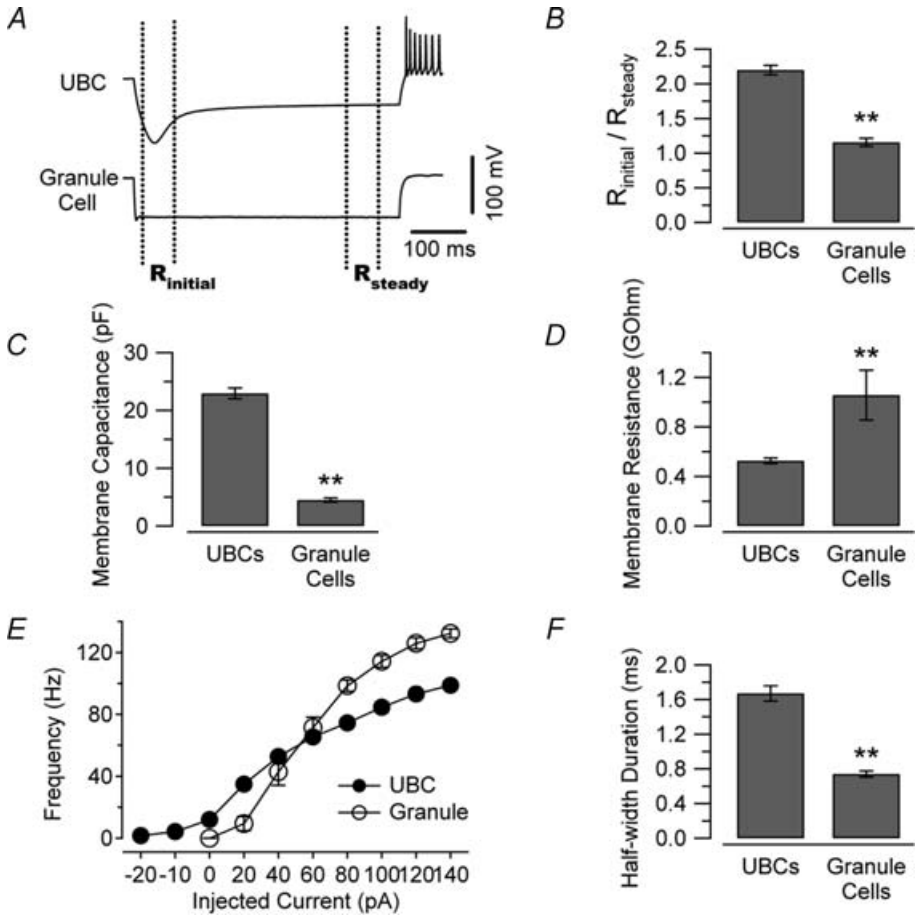


**Figure 2. Intrinsic properties of UBCs and granule cells**
*A*, voltage traces recorded in a UBC (upper trace) and a GC (lower trace) in response to hyperpolarizing current injection (−200 pA, 500 ms). The dotted lines depict the trace segments used for the determination of peak and steady state input resistance. *B*, bar chart comparing the ratio of the peak to steady state input resistance in 58 UBCs and 15 GCs. *C* and *D*, UBCs were also characterized by considerably larger capacitance and lower input resistance (*D*, measured at steady state). *E*, input/output relation for the two cell types. The firing frequency curve was considered saturated when spikes after the first one were not overshooting (did not reach 0 mV). Contrary to GCs, UBCs are intrinsically firing, as can be noted by the non-zero origin of their *F–I* curve. Note also the higher maximum frequency reached by GCs. *F*, the spike half-duration also differed between the two cell types. The values shown in the bar charts were recorded in response to injections of 40 pA of current, which produced similar firing frequencies in the two cell types (see panel *E*). In the plot of panel *E*, error bars are within the symbols. (**$P < 0.01$.)

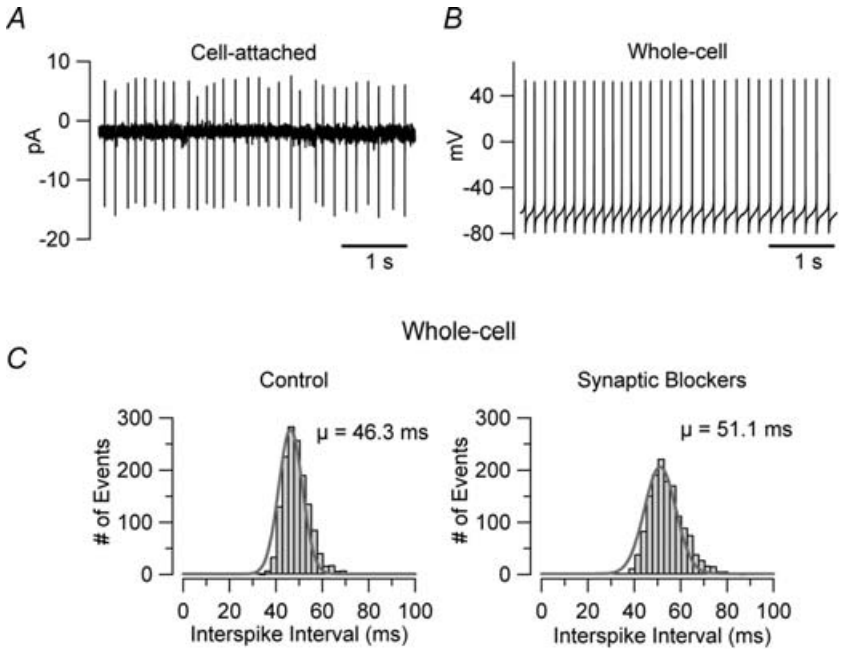


**Figure 3. UBCs are intrinsically firing**
*A*, cell-attached recording from a UBC in an acute slice at 21–23°C. The pipette solution consisted of Hepes-buffered artificial cerebrospinal fluid (containing 2.5 mM KCl). *B*, another cell, recorded in whole cell configuration with K-gluconate internal solution, shows similar firing frequency. *C*, the firing was independent of synaptic stimulation. The bar charts show the interspike interval from an individual cell in control conditions and after application of blockers of fast synaptic transmission (2 mM kynurenic acid and 0.1 mM picrotoxin).

is shown in Fig. 8. Although the size of the TTX-sensitive sodium current during the interspike interval (Fig. 8*D*) was quite small (the average value was $-1.6 \pm 0.5$ pA at $-72$ mV, $n = 4$), it represented ∼1% of the total sodium current in the patch, a value considerably larger than in other intrinsically firing neurons (Taddese & Bean, 2002; Jackson *et al.* 2004). This suggests that the properties of the UBC's sodium current are tuned to sustain intrinsic firing. The sodium current, however, was not the only current active during the interspike interval. We noticed that also when the extracellular solution contained the full cocktail of blockers of voltage-gated currents (100 $\mu$M cadmium or equiosmolar calcium substitution with cobalt, 3 mM Cs, 20 mM TEA, and 300 nM TTX), an inward current

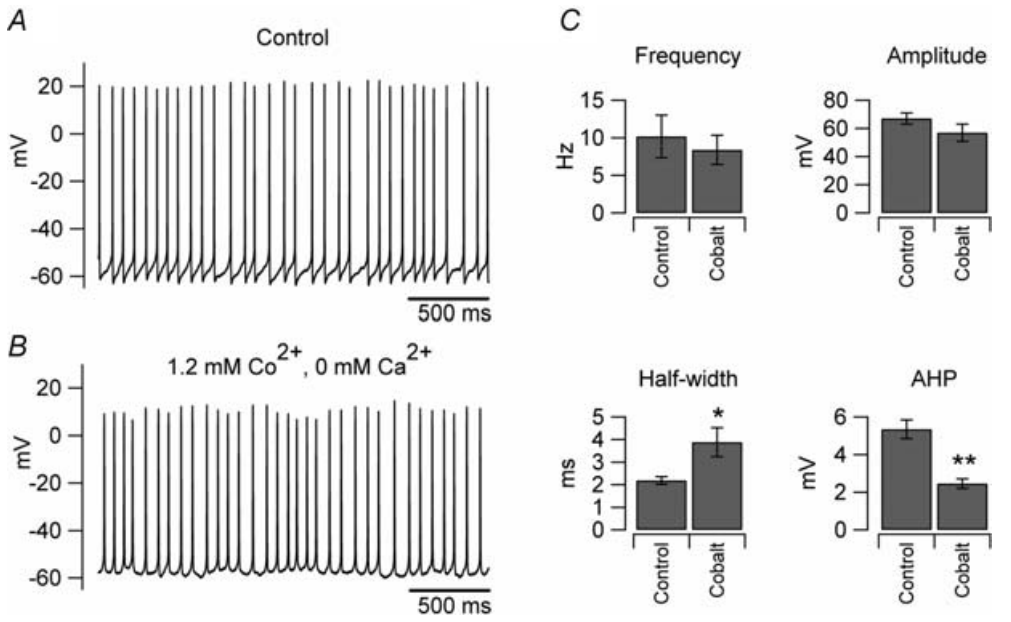


**Figure 4. Intrinsic firing is unaffected by calcium replacement with cobalt**
*A*, trace recorded in an individual UBC when the extracellular solution consisted of standard ACSF (1.2 mM $Ca^{2+}$). *B*, the same cell recorded after extracellular calcium was replaced by equimolar concentration of cobalt. *C*, comparison of the average firing parameters obtained from 8 cells in the two conditions. Two parameters were significantly affected by cobalt substitution: the spike half-duration, which increased by 75% and the amplitude of the after-hyperpolarization (AHP), which decreased by 52% (*$P < 0.05$, **$P < 0.01$).

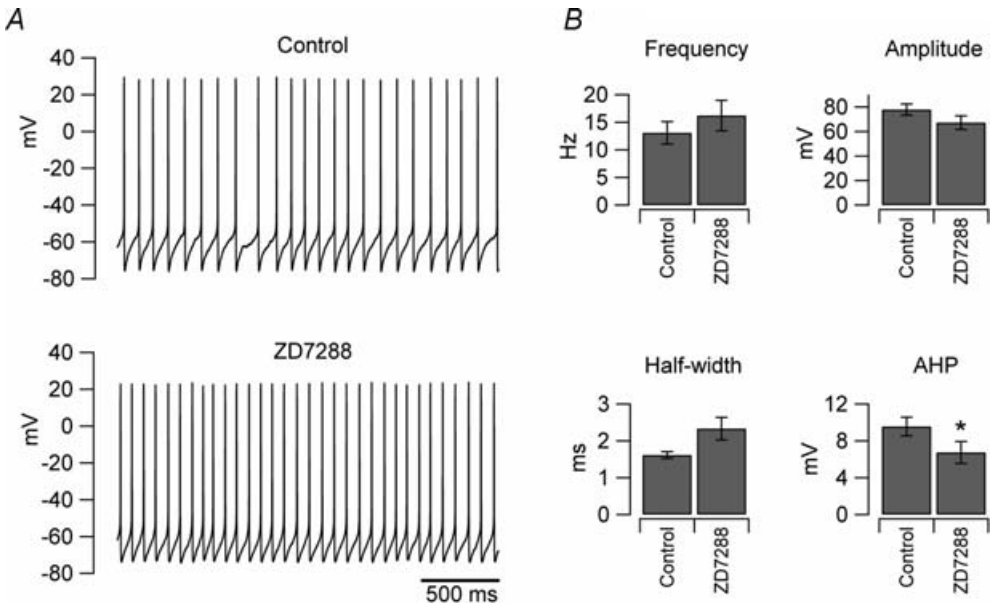


**Figure 5. ZD7288 does not affect intrinsic firing of UBCs**
*A*, traces recorded from an individual UBC in control condition (upper trace) and in the presence of $I_h$ blocker ZD7288 (lower trace). No significant differences in the firing frequency were observed (paired *t* test, $P > 0.05$). *B*, bar charts showing the average effects of the drug on the firing properties in 8 neurons; notice that there was no decrease of the firing frequency (paired *t* test, $P > 0.05$).

during the interspike interval could still always be detected (Fig. 8*E*). This current had an average size of $-9.9 \pm 6.3$ pA (at $-72$ mV, $n = 10$). In order to exclude that such current was simply the result of a leakage through an imperfect seal, we tested whether it could be blocked by substitution of extracellular sodium with the channel-impermeable cation *N*-methyl-D-glucamine (NMDG). Figure 8*E* shows that NMDG blocked the inward current almost completely (the NMDG current at $-90$ mV was 7% of the control value), thus suggesting that it was not a recording artifact.

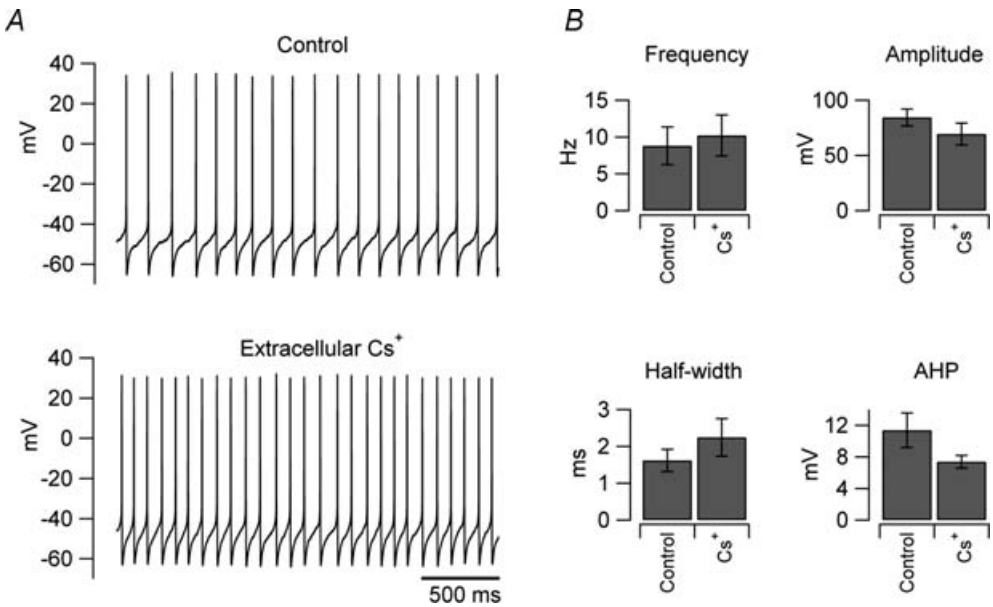


**Figure 6. Extracellular caesium does not affect Intrinsic firing of UBCs**
*A*, traces recorded from an individual UBC in control condition (upper trace) and in the presence of extracellular caesium (3 mM, lower trace). *B*, bar charts showing the average effects of the drug on the firing properties in 3 neurons; no significant differences in the firing frequency were observed (paired *t* test, $P > 0.05$).

In these recordings the cationic current was considerably larger than the persistent sodium current; this, however, could reflect the clustering of sodium channels in compartments other than the soma. In order to obtain a better estimate of the size of persistent sodium current in UBCs, we studied the effect of TTX on the input resistance. Both voltage-clamp (not shown) and current-clamp recordings (Fig. 9*A*), showed that TTX induced a large increase of the input resistance (94 ± 41% at −82 mV, $n = 6$, Fig. 9*B*), confirming that TTX sensitive sodium channels are open at rest. Assuming a simple equivalent circuit in which the TTX-sensitive conductance is in parallel with another conductance, calculations show that at −70 mV the estimated persistent sodium current is ∼100 pA.

These results suggest that TTX-sensitive sodium and cationic current both drive intrinsic firing of UBCs. If this is the case, application of TTX at non-saturating concentrations could still allow spontaneous firing. Application of 10 nM TTX, which blocks roughly 50% of the sodium currents in central mammalian neurons (Madeja, 2000), decreased the frequency from 7.7 ± 1.8 Hz to 6.8 ± 1.3 Hz ($n = 5$, Fig. 9*C* and *D*) but did not prevent intrinsic firing (although it induced a significant decrease of the spike amplitude, Fig. 9*E*). These data further suggest that the TTX-sensitive current may not be the only current to bring the neurons to threshold. For all the experiments shown in Fig. 9 strychnine (1 μM) was also added to both the control and the TTX solutions in order to exclude secondary effects due to the possible removal of the glycinergic inputs to UBCs (Dugué *et al.* 2005).

These results support the hypothesis that the TTX-sensitive sodium current and an unselective cationic current are both necessary for bringing the membrane potential to firing threshold.

### Properties of the cationic background current

So far, we have shown that in UBCs a cationic current is present during the interspike intervals in addition to the TTX-sensitive sodium current, and therefore appears to play a role in driving the intrinsic firing of these neurons.

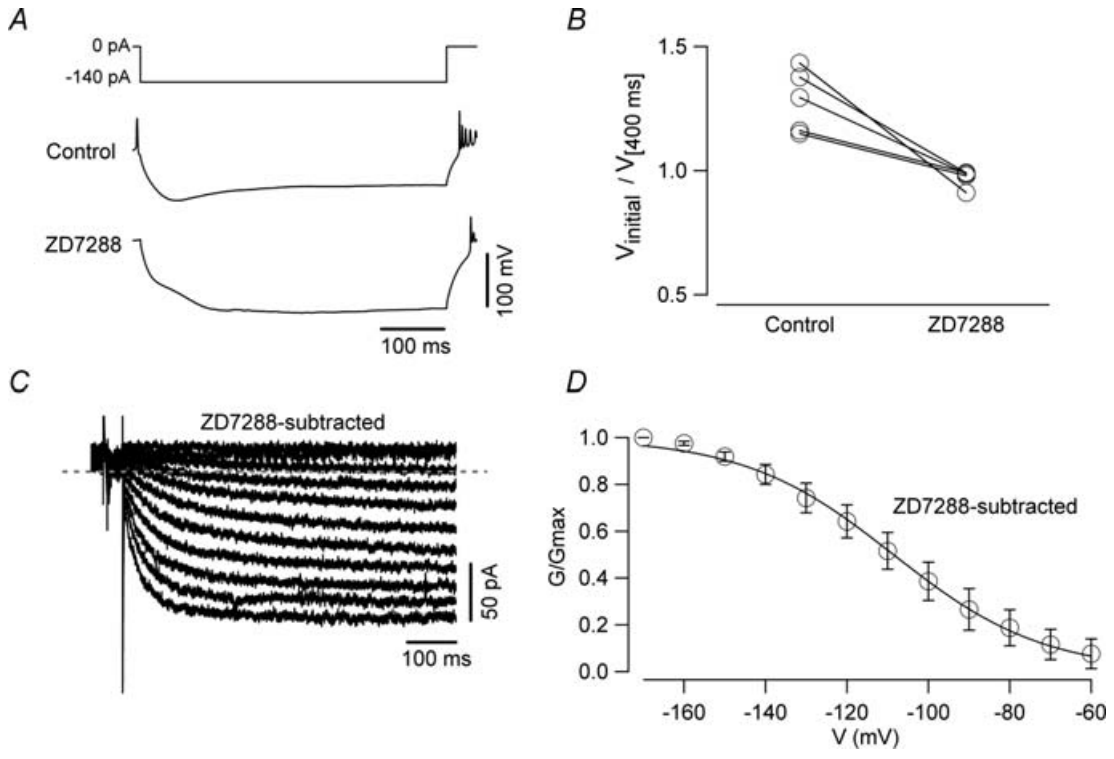


**Figure 7. ZD7288 effectively blocks Ih in UBCs**
*A*, whole-cell current clamp recordings showing the voltage response of a UBC to a 500 ms hyperpolarizing current injection (top trace) in control condition (middle trace) and in the presence of ZD7288 (100 μM, lower trace). Note that ZD7288 completely abolished the voltage sag. *B*, plot showing the effects of ZD7288 on the ratio of the value of membrane potentials measured at peak and after 400 ms in 5 UBCs. The voltage sag was abolished completely by the drug. *C*, voltage-clamp recording of the ZD-sensitive current. The traces were obtained by digital subtraction of the current recorded in ZD7288 from that recorded in control conditions. *D*, conductance–voltage relationship of the ZD-sensitive current. No activation was detected for membrane potential values positive to −60 mV.

To further characterize this current, voltage-clamp recordings were obtained from nucleated patches after pharmacological blockade of voltage gated currents. Calcium channels were blocked either by substituting cobalt for calcium or by addition of 0.1 mM cadmium to the bath; 3 mM caesium was applied to block inward rectifier potassium currents and $I_h$, and TEA (20 mM) to block voltage-gated potassium currents; TTX 300 nM was used to block sodium currents. Figure 10*A* shows traces recorded under these conditions in response to short 10 mV voltage steps from a holding potential of −72 mV. At this holding potential an inward current was always detected. In this patch, the current reversed at ∼−40 mV and exhibited linear *I–V* relation for potentials negative to − 40 mV. Substitution of external sodium with NMDG resulted in the almost complete suppression of the inward current and led to a shift of the reversal potential by ∼45 mV (Fig. 10*A* and *B*), suggesting that the current is mediated by a mix of sodium and potassium ions. Because of the possible contamination of this current by TEA- and caesium-insensitive potassium conductances, as suggested by the quite negative reversal potential and the deviation from linearity at more depolarized potentials, the reversal potential of the cationic current was further examined by performing experiments using a CsCl internal solution. The recordings, obtained in whole cell configuration, were also performed in the presence of TTX, cobalt, caesium and TEA (Fig. 10*D*). Currents were normalized to the current recorded at −100 mV and averaged. The resulting *I–V* relation (obtained from 5 cells, Fig. 10*E*) was linear over the potentials examined and showed a reversal potential of ∼−25 mV, suggesting a low selectivity among cations.

What could be the nature of this current? It has been recently shown in cerebellar slice recordings that tonic ATP release stimulates spontaneous activity of molecular layer interneurons (Casel *et al.* 2005). To assess the presence of a background purinergic current in UBCs we bath applied suramin, a non-specific P2 receptor antagonist (North & Surprenant, 2000; von Kugelgen, 2006). Suramin (100 μM,

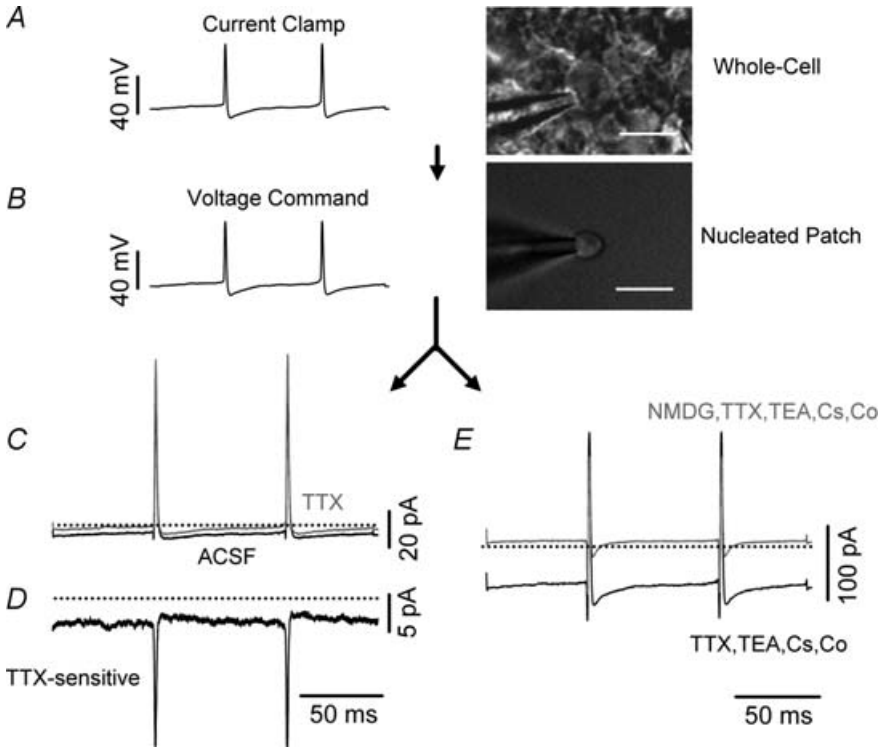


**Figure 8. Wave-clamp recordings reveal two distinct inward currents during the interspike interval**
Wave clamp recordings from nucleated patches were used to identify the currents driving the intrinsic firing of UBCs. *A*, voltage recordings were obtained in whole cell configuration, and then used as voltage commands (*B*) for nucleated patches obtained from the same cells. *C*, current recordings from a nucleated patch in control condition (ACSF, darker line) and in the presence of TTX 300 nM. *D*, the TTX-sensitive current obtained by digital subtraction of the trace in TTX from the control trace. *E*, In the same patch, a large cationic inward current was recorded when cobalt was substituted for calcium and $Cs^+$ (3 mM) TTX (300 nM) and TEA (20 mM) were added in order to block voltage-gated currents. In this condition, the net inward current was actually larger than in control, most likely because a steady potassium current was blocked. The inward current, however, was not a recording artifact as indicated by the fact that it was almost completely blocked upon replacement of extracellular sodium and potassium by NMDG-Cl ($n = 10$). Calibration bars = 5 μm.

not shown), however, did not affect the firing frequency of UBCs nor the cells' input resistance.

A widely expressed family of cationic channels is the TRP. Ruthenium red is a wide spectrum blocker of channels belonging to this family (Guler *et al.* 2002; Nagata *et al.* 2005). As shown in Fig. 11*A*, when bath applied, ruthenium red (0.1 mM) blocked a considerable fraction ($71 \pm 4\%$) of the subthreshold current. The ruthenium red-sensitive current was voltage independent and had a reversal potential $\sim -18$ mV in our experimental conditions (Fig. 11*B*). Bath application of ruthenium red, however, was not sufficient to stop intrinsic firing. We reasoned that this fact could arise from the increased efficacy of the TTX-sensitive sodium current due to the higher input resistance of the cells in the presence of ruthenium red. If so, reducing the sodium channel current should unmask the effect of the cationic current on firing. Therefore, we first bath applied 10 nM TTX, which – in this set of experiments – reduced the firing frequency by 41%, and then tested the effect of the cationic current blockade under this condition. Application of ruthenium red in the presence of TTX strongly decreased the firing frequency (from $11.1 \pm 2.8$ Hz to $2.2 \pm 0.8$ Hz, $n = 4$, $P < 0.05$, Fig. 11*C* and *D*), confirming a role for the cationic current in the intrinsic firing of UBCs. In three of the four cells tested the effect of ruthenium red on the firing frequency was partly reversible upon washout (the frequency after washout of ruthenium red was $4.7 \pm 1.1$ Hz, $n = 4$, Fig. 11*D*).

## Discussion

Our results show that the electrophysiological properties of the UBCs clearly differentiate them from neighbouring granule cells. UBCs have larger capacitance and show strong voltage sag in response to large hyperpolarization; moreover, UBCs are intrinsically firing. The analysis of the mechanisms of intrinsic firing showed that it is likely to be driven by a TTX-sensitive sodium current in combination with a

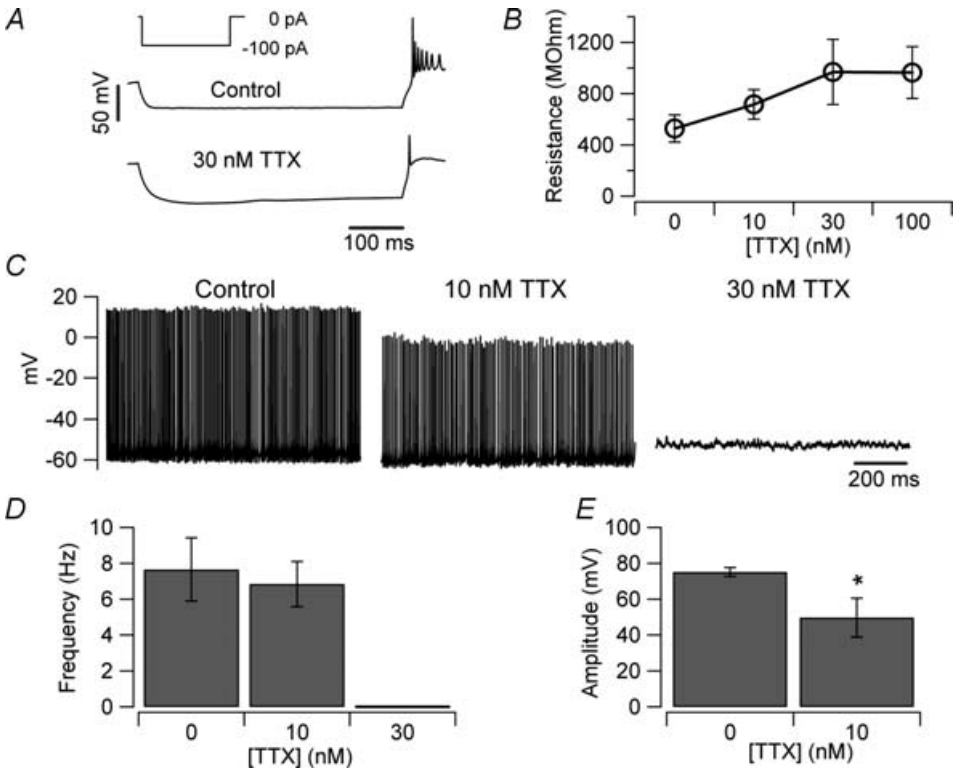


**Figure 9. Effects of TTX on firing and intrinsic properties**
*A*, current clamp recordings showing the voltage response of a UBC to hyperpolarizing current injection (inset) in control (upper trace) and in the presence of 30 nM TTX (lower trace). When the persistent sodium current was blocked by TTX, the current injection induced a much larger voltage response that could activate $I_h$. *B*, plot of the input resistance value *versus* TTX concentration (the input resistance was measured in voltage clamp, by delivering 5 ms long 10 mV pulses from a holding potential of −80 mV). *C*, recording of the intrinsic firing of a UBC in the presence of kynurenic acid, picrotoxin and strychnine (no holding current was injected). Addition of 10 nM TTX to the bath reduced, but did not stop, firing. A higher TTX concentration (30 nM) completely abolished intrinsic firing and set the membrane potential of the neurons at $-53 \pm 6$ mV ($n = 5$). *D*, bar chart showing the average effect of TTX on the firing frequency of UBCs ($n = 5$). *E*, 10 nM TTX significantly decreased the UBC spike amplitude (*$P < 0.05$).

TTX-insensitive, voltage-independent, TRP-like cationic current.

### Intrinsic properties of UBCs and granule cells

UBCs and granule cells are two types of glutamategic cerebellar interneurons situated in the granular layer and impinged upon by mossy fibres (Mugnaini *et al.* 1994; Rossi *et al.* 1995; Nunzi *et al.* 2001). Albeit both neuronal types have very small cell bodies, they differ in average diameter by a few micrometres (Mugnaini & Floris, 1994). The difference in membrane capacitance of these cell types, however, is quite large (Dugué *et al.* 2005; Forti *et al.* 2006; this paper). The capacitance values are distributed quite narrowly around the respective means with virtually no overlap. Thus a simple capacitance measurement can distinguish between the two cell types almost certainly. Most likely, the much larger capacitance of the UBCs is due to the extensive surface of the brush. The capacitance value also allows to easily distinguish UBCs from Golgi cells, which have a much larger capacitance (about 5 times larger, Dieudonné, 1998; Forti *et al.* 2006). Functionally, the more obvious difference between UBCs and granule cells is represented by the fact that UBCs are spontaneously firing. However, the differences between these two types of neuron extend also to the firing patterns recorded in response to current injections. The maximum firing frequency of granule cells is considerably higher than in UBCs, possibly because granule cells have larger resurgent current than UBCs (Afshari *et al.* 2004). Interestingly, among the four cell types examined by Afshari *et al.* the UBCs were the cell type with the lowest ratio of resurgent current to transient current, whereas granule cells had a ratio very close to that of Purkinje neurons, which are capable of spiking at extremely high rates both *in vitro* and *in vivo* (Latham & Paul, 1971; Raman &

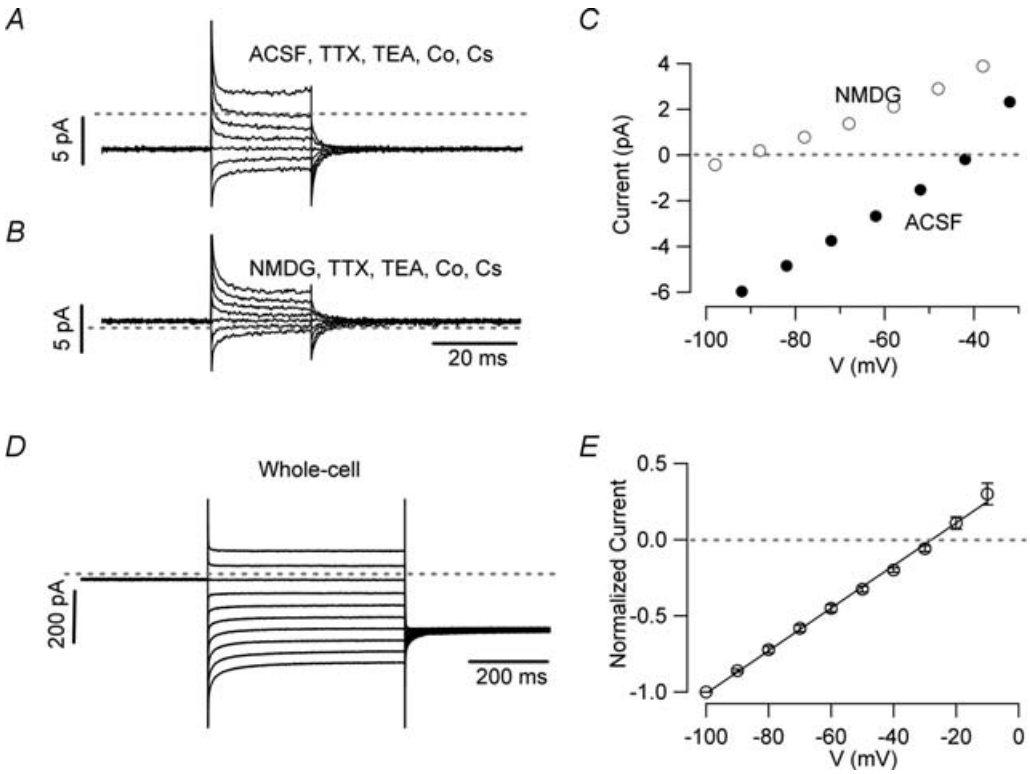


**Figure 10. Properties of the leakage current**
*A*, current traces recorded in the presence of voltage-gated channels blockers in a nucleated patch in response to 25 ms voltage pulses from −92 to −32 mV. *B*, substitution of extracellular sodium and potassium with NMDG caused the steady current at −72 mV to shift from inward to outward. *C*, *I–V* relations of the traces in *A* and *B*. Data points recorded in the NMDG-based solution were corrected for liquid junction potential (6 mV) of this solution relative to control. Note the ∼40 mV shift of the reversal potential and the almost complete block of the inward component, as expected for a cationic current. *D*, whole-cell voltage-clamp recording obtained from a UBC using a CsCl intracellular solution in the presence of voltage-gated channel blockers. Cells were held at −60 mV. The step protocol was preceded by a prepulse to −20 mV to inactivate voltage-gated currents that might have proved resistant to pharmacological block. After the pulses, the membrane potential was returned to the holding value. *E*, current–voltage relationship obtained from 5 cells. The reversal potential of the current was −25 mV.

Bean, 1999; Häusser & Clark, 1997; McKay *et al.* 2005). However, it is well known that the properties of potassium currents are as important as those of sodium currents in enabling fast spiking (reviewed by Rudy & McBain, 2001). The observed differences in half-duration of the spike could suggest that potassium currents also differ in the two cell types. Further studies will be required to address the properties of potassium currents in UBCs. Another large difference between UBCs and granule cells appears in response to hyperpolarizing current injections. At negative membrane potentials, UBCs always present a voltage sag, which is negligible in granule cells. Thus, the expression of $I_h$ also appears to differ between these cell types. However, in spite of its prominence in UBCs, $I_h$ did not contribute to intrinsic firing, probably because it activated at voltages that were more hyperpolarized than those associated with autonomous activity, similar to what was described for substantia nigra pars reticulata neurons (Atherton & Bevan, 2005). On the contrary, $I_h$ blockers unexpectedly tended to increase the firing frequency of UBCs. The most likely explanation is that these effects were due to actions of the blockers on currents other than $I_h$. ZD7288 has been reported to substantially block voltage-gated potassium currents (Do & Bean, 2003), and caesium blocks the inward rectifier current, which is expressed in UBCs (Harashima *et al.* 2006).

### Mechanisms of intrinsic firing

**Methodological considerations.** The mechanisms of intrinsic firing have typically been studied by testing the effect of blockers of several currents in current clamp. However, the interpretation of such data can be difficult because the blockade of a current responsible for the firing always results in the change of the voltage trajectory of the spikes, thus affecting also all the other voltage-gated channels present in the membrane. On the other hand, more direct methods, such as the action potential clamp

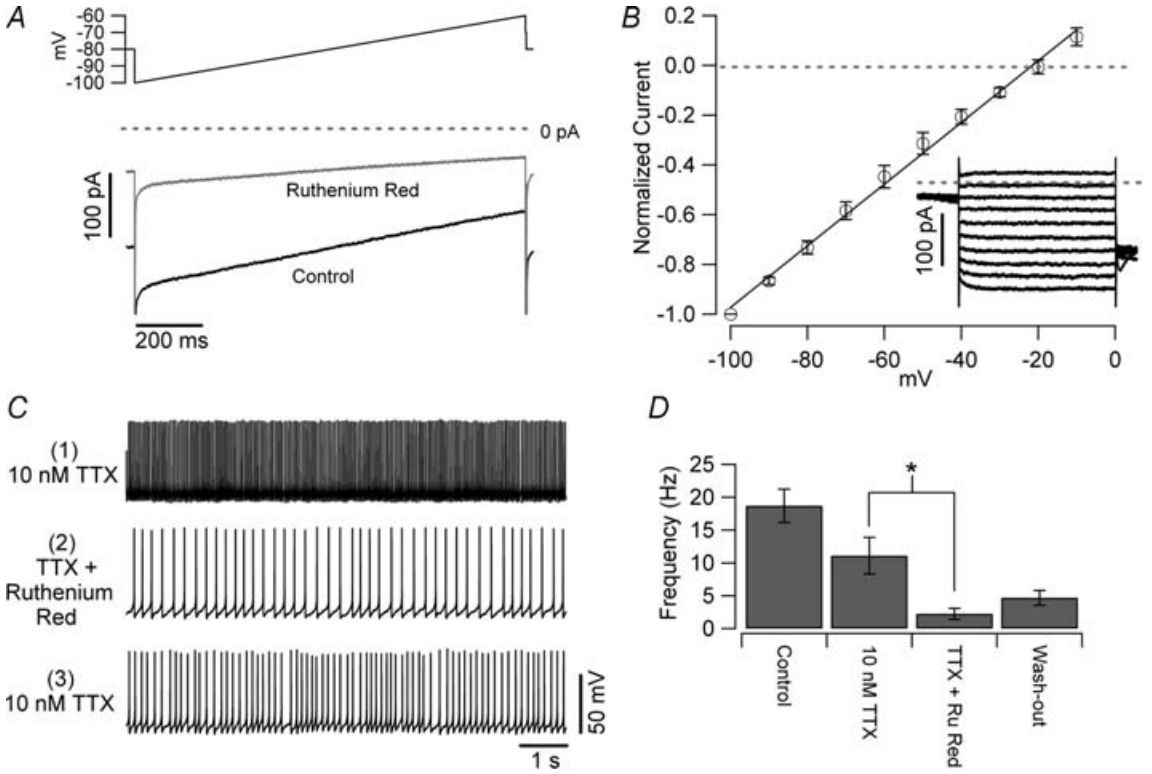


**Figure 11. Effects of ruthenium red on UBCs**
*A*, whole-cell voltage-clamp recording obtained from a UBC with caesium-based intrapipette solution in response to a slow voltage ramp (0.03 mV $ms^{-1}$, upper trace). The current (control, lower trace) was recorded in an extracellular solution containing 2 mM caesium, 5 mM TEA, 300 nM TTX and in which calcium was completely substituted by cobalt. Note the strong blockade induced by ruthenium red (0.2 mM, middle trace). *B*, *I–V* relationship of the ruthenium-red sensitive current. The inset shows the current traces (obtained by digital subtraction) recorded in response to 10 mV steps from −100 to 0 mV. *C*, current clamp recordings of intrinsically firing UBCs obtained in the presence of normal ACSF plus synaptic blockers and 10 nM TTX (upper trace). Under these conditions, ruthenium red consistently reduced the firing frequency (middle trace and panel *D*). The effect of ruthenium red was partially reversible upon wash-out in 3 of 4 cells; in the washout condition (lower trace and panel *D*), only ruthenium red was omitted, and cells were still bathed in TTX.

(Llinás *et al.* 1982; de Haas, 1989), require optimal voltage-clamp conditions, which are not achievable in slice recordings. We have combined whole-cell current-clamp recordings in slice with nucleated patch recordings in which the voltage command was provided by the spikes previously recorded in whole-cell from the very same neurons. Thus, we could combine current-clamp recordings from identified cells in slices to voltage-clamp recordings in almost ideal clamp conditions (Martina & Jonas, 1997; Baranauskas & Martina, 2006). Obviously, this method has limitations too; one is that nucleated patches do not usually comprise axon and dendrites, and consequently have lower sodium channel density than whole cells recorded in slice or even acutely dissociated neurons. Thus, although the UBC has an extremely short dendrite and therefore represents a system in which nucleated patches are more representative of the intact cell situation than for most other neurons, the relative amplitude of the sodium and the TRP-like current recorded during the interspike intervals should still be interpreted cautiously because of the likely clustering of sodium currents in non-somatic compartments.

**The nature of the interspike current of UBCs.** Current-clamp recordings showed that blockade of calcium currents by replacement of calcium with cobalt did not have any detectable effect on the intrinsic firing frequency of UBCs. Blockade of $I_h$ current either by caesium or by ZD7288 also produced no significant effect, in agreement with the observation that the voltage sag observed in response to current injections appears at membrane potentials more negative than those experienced during tonic firing.

These data suggested that, similarly to tuberomammilary (Taddese & Bean, 2002) and subthalamic nucleus neurons (Do & Bean, 2003), the current responsible for the intrinsic firing of UBCs could be mediated mainly by TTX-sensitive sodium channels. Wave-clamp recordings confirmed the presence of TTX-sensitive current during interspike intervals, although it was not the only current in this phase of the spiking cycle. A voltage-independent, cationic, inward current was also always detected during the interspike interval, and thus contributed to the drive toward firing threshold.

What can be the molecular basis of this current? The voltage-independent cationic channels most commonly expressed in the nervous system belong to the TRP family. In agreement with the possibility that such channels contribute to the cationic current, ruthenium red blocked about 70% of the current. In the presence of low concentration of TTX, ruthenium red promptly and reversibly reduced the firing frequency (in one cell it completely and reversibly abolished firing).

It is interesting that when intrinsic firing was blocked by TTX UBCs had a resting potential of $\sim -55$ mV, which is less positive than could be expected on the basis of the relatively large cationic current. This difference could be explained by the persistent activation of potassium conductances. For instance, it could be suggested that in nonsomatic compartments of the UBCs (such as the brush), potassium-selective leak channels could be expressed together with the non-selective cationic channels. These hypotheses are supported by the fact that UBCs express G protein-coupled inwardly rectifying potassium currents (GIRK, Knoflach & Kemp, 1998) and by recent data showing that GIRK2 expression in UBCs is particularly strong in the brush (Harashima *et al.* 2006).

**Low specific membrane resistance and intrinsic firing.** UBCs are small neurons with a capacitance of $\sim$20 pF. Nevertheless, these cells have relatively low input resistance ($\sim$500 M$\Omega$). These values correspond to a specific membrane resistance of $\sim$11 k$\Omega$ cm$^2$. This value is quite low compared to typical neuronal types such as hippocampal pyramidal cells (25–27 k$\Omega$ cm$^2$; Antic, 2003; Taverna *et al.* 2005), hippocampal OLM interneurons (48 k$\Omega$ cm$^2$; Taverna *et al.* 2005) and, particularly, intrinsically firing neurons as the Golgi cells ($\sim$85 k$\Omega$ cm$^2$, calculated from the data reported in Forti *et al.* 2006). This observation leads to two distinct considerations. First, the leakage current of UBCs does not appear to be primarily mediated by members of the KCNK family, contrary to most other neuronal types (Millar *et al.* 2000; Talley *et al.* 2000; Meuth *et al.* 2003; Taverna *et al.* 2005), because a high density of such channels would effectively prevent intrinsic firing by maintaining the membrane potential at more hyperpolarized levels. Second, the low input resistance implies that, although the UBCs are small cells, the current needed to effectively drive intrinsic firing must be considerably larger than the few picoamperes that are sufficient to drive the firing of high input resistance neurons (Taddese & Bean, 2002; Jackson *et al.* 2004). Thus, the TTX-sensitive sodium current flowing between spikes, although quite large in proportion to the total sodium current, might not be sufficient for the task. Because neither $I_h$ nor voltage-gated calcium currents seem to contribute to intrinsic firing in these cells, the current active during the interspike intervals might be the same TRP-like current that is also responsible for the low input resistance.

The combination of high input resistance with the standard biophysical properties of mammalian neuronal sodium channels (Taddese & Bean, 2002) appears to be ideally suited to ensure intrinsic firing in small neurons. Yet, contrary to other small neurons, UBCs have developed a mechanism for intrinsic firing that accommodates their remarkably low specific membrane resistance. What could be the reason for this difference?

One possible answer could be found in the peculiar synaptic response of UBCs to synaptic excitation (Rossi *et al.* 1995). Due to the anatomical properties of the mossy fibre–UBC synapse, the glutamatergic response of the UBCs is unusually long-lasting. In a high input resistance neuron, such currents could result in extreme depolarizations and complete inactivation of voltage-gated sodium and potassium channels. In UBCs from young rats, on the other hand, these prolonged excitatory synaptic potentials did not result in extreme depolarizations but rather generated bursts of high frequency spikes (Rossi *et al.* 1995). UBC properties could alternatively be related to the developmental history of these neurons. It has been speculated that UBCs constitute a subclass of cerebellar nuclear neurons that migrate up to the cortex during development, bringing to mind the piscine cerebellar eurydendroid cells (Mugnaini & Floris, 1994; Ilijic *et al.* 2005). Interestingly, presumed glutamatergic neurons of the cerebellar nuclei have also been shown to rely on a combination of unspecific cationic currents and TTX-sensitive persistent current to achieve spontaneous firing (Raman *et al.* 2000).

Finally, it is notable that the cerebellum is endowed with a particularly high number of intrinsically firing neuronal types. Indeed, UBCs, Purkinje neurons (Gruol & Franklin, 1987; Raman & Bean, 1999), molecular layer interneurons (basket and stellate cells, Häusser & Clark, 1997; Carter & Regehr, 2002), cerebellar nuclei neurons (Raman *et al.* 2000; Molineux *et al.* 2006), and Golgi cells (Forti *et al.* 2006) all are capable of autorhythmic firing. The reason for this peculiarity of the cerebellar network remains unclear, but it could be suggested that this background activity allows a quicker response of the system to external inputs.

## References


Afshari FS, Ptak K, Khaliq ZM, Grieco TM, Slater NT, McCrimmon DR & Raman IM (2004). Resurgent Na currents in four classes of neurons of the cerebellum. *J Neurophysiol* **92**, 2831–2843.

Antic SD (2003). Action potentials in basal and oblique dendrites of rat neocortical pyramidal neurons. *J Physiol* **550**, 35–50.

Atherton JF & Bevan MD (2005). Ionic mechanisms underlying autonomous action potential generation in the somata and dendrites of GABAergic substantia nigra pars reticulata neurons in vitro. *J Neurosci* **25**, 8272–8281.

Bal T & McCormick DA (1993). Mechanisms of oscillatory activity in guinea-pig nucleus reticularis thalami in vitro: a mammalian pacemaker. *J Physiol* **468**, 669–691.

Baranauskas G & Martina M (2006). Sodium currents activate without a Hodgkin-and-Huxley-type delay in central mammalian neurons. *J Neurosci* **26**, 671–684.

Bevan MD & Wilson CJ (1999). Mechanisms underlying spontaneous oscillation and rhythmic firing in rat subthalamic neurons. *J Neurosci* **19**, 7617–7628.

Billups D, Liu YB, Birnstiel S & Slater NT (2002). NMDA receptor-mediated currents in rat cerebellar granule and unipolar brush cells. *J Neurophysiol* **87**, 1948–1959.

Brown H & DiFrancesco D (1980). Voltage-clamp investigations of membrane currents underlying pace-maker activity in rabbit sino-atrial node. *J Physiol* **308**, 331–351.

Carter AG & Regehr WG (2002). Quantal events shape cerebellar interneuron firing. *Nat Neurosci* **5**, 1309–1318.

Casel D, Brockhaus J & Deitmer JW (2005). Enhancement of spontaneous synaptic activity in rat Purkinje neurones by ATP during development. *J Physiol* **568**, 111–122.

Cauli B, Audinat E, Lambolez B, Angulo MC, Ropert N, Tsuzuki K, Hestrin S & Rossier J (1997). Molecular and physiological diversity of cortical nonpyramidal cells. *J Neurosci* **17**, 3894–3906.

de Haas & Vogel W (1989). Sodium and potassium currents recorded during an action potential. *Eur Biophys J* **17**, 49–51.

Dieudonné S (1998). Submillisecond kinetics and low efficacy of parallel fibre-Golgi cell synaptic currents in the rat cerebellum. *J Physiol* **510**, 845–866.

DiFrancesco D (1981). A study of the ionic nature of the pace-maker current in calf Purkinje fibres. *J Physiol* **314**, 377–393.

Do MT & Bean BP (2003). Subthreshold sodium currents and pacemaking of subthalamic neurons: modulation by slow inactivation. *Neuron* **39**, 109–120.

Dugué GP, Dumoulin A, Triller A & Dieudonné S (2005). Target-dependent use of co-released inhibitory transmitters at central synapses. *J Neurosci* **25**, 6490–6498.

Feigenspan A, Gustincich S, Bean BP & Raviola E (1998). Spontaneous activity of solitary dopaminergic cells of the retina. *J Neurosci* **18**, 6776–6789.

Forti L, Cesana E, Mapelli J & D'Angelo E (2006). Ionic mechanisms of autorhythmic firing in rat cerebellar Golgi cells. *J Physiol* **574**, 711–729.

Freund TF & Buzsáki G (1996). Interneurons of the hippocampus. *Hippocampus* **6**, 347–470.

Gruol DL & Franklin CL (1987). Morphological and physiological differentiation of Purkinje neurons in cultures of rat cerebellum. *J Neurosci* **7**, 1271–1293.

Guler AD, Lee H, Iida T, Shimizu I, Tominaga M & Caterina M (2002). Heat-evoked activation of the ion channel, TRPV4. *J Neurosci* **22**, 6408–6414.

Harashima C, Jacobowitz DM, Stoffel M, Chakrabarti L, Haydar TF, Siarey RJ & Galdzicki Z (2006). Elevated expression of the G-protein-activated inwardly rectifying potassium channel 2 (GIRK2) in cerebellar unipolar brush cells of a Down Syndrome mouse model. *Cell Mol Neurobiol* **26**, 717–732.

Häusser M & Clark BA (1997). Tonic synaptic inhibition modulates neuronal output pattern and spatiotemporal synaptic integration. *Neuron* **19**, 665–678.

Ilijic E, Guidotti A & Mugnaini E (2005). Moving up or moving down? Malpositioned cerebellar unipolar brush cells in reeler mouse. *Neuroscience* **136**, 633–647.

Jackson AC, Yao GL & Bean BP (2004). Mechanism of spontaneous firing in dorsomedial suprachiasmatic nucleus neurons. *J Neurosci* **24**, 7985–7998.

Jones HC & Keep RF (1988). Brain fluid calcium concentration and response to acute hypercalcaemia during development in the rat. *J Physiol* **402**, 579–593.

Kinney GA, Overstreet LS & Slater NT (1997). Prolonged physiological entrapment of glutamate in the synaptic cleft of cerebellar unipolar brush cells. *J Neurophysiol* **78**, 1320–1333.

Knoflach F & Kemp JA (1998). Metabotropic glutamate group II receptors activate a G protein-coupled inwardly rectifying $K^+$ current in neurones of the rat cerebellum. *J Physiol* **509**, 347–354.

Latham A & Paul DH (1971). Spontaneous activity of cerebellar Purkinje cells and their responses to impulses in climbing fibres. *J Physiol* **213**, 135–156.

Lien CC, Martina M, Schultz JH, Ehmke H & Jonas P (2002). Gating, modulation and subunit composition of voltage-gated $K^+$ channels in dendritic inhibitory interneurones of rat hippocampus. *J Physiol* **538**, 405–419.

Llinás R (1988). The intrinsic electrophysiological properties of mammalian neurons: insights into central nervous system function. *Science* **242**, 1654–1664.

Llinás R, Sugimori M & Simon SM (1982). Transmission by presynaptic spike-like depolarization in the squid giant synapse. *Proc Natl Acad Sci U S A* **79**, 2415–2419.

Madeja M (2000). Do neurons have a reserve of sodium channels for the generation of action potentials? A study on acutely isolated CA1 neurons from the guinea-pig hippocampus. *Eur J Neurosci* **12**, 1–7.

Martina M & Jonas P (1997). Functional differences in $Na^+$ channel gating between fast-spiking interneurones and principal neurones of rat hippocampus. *J Physiol* **505**, 593–603.

Martina M, Schultz JH, Ehmke H, Monyer H & Jonas P (1998). Functional and molecular differences between voltage-gated $K^+$ channels of fast-spiking interneurons and pyramidal neurons of rat hippocampus. *J Neurosci* **18**, 8111–8125.

Martina M, Vida I & Jonas P (2000). Distal initiation and active propagation of action potentials in interneuron dendrites. *Science* **287**, 295–300.

McKay BE, Molineux ML, Mehaffey WH & Turner RW (2005). Kv1 $K^+$ channels control Purkinje cell output to facilitate postsynaptic rebound discharge in deep cerebellar neurons. *J Neurosci* **25**, 1481–1492.

Meuth SG, Budde T, Kanyshkova T, Broicher T, Munsch T & Pape HC (2003). Contribution of TWIK-related acid-sensitive $K^+$ channel 1 (TASK1) and TASK3 channels to the control of activity modes in thalamocortical neurons. *J Neurosci* **23**, 6460–6469.

Millar JA, Barratt L, Southan AP, Page KM, Fyffe RE, Robertson B & Mathie A (2000). A functional role for the two-pore domain potassium channel TASK-1 in cerebellar granule neurons. *Proc Natl Acad Sci U S A* **97**, 3614–3618.

Molineux ML, McRory JE, McKay BE, Hamid J, Mehaffey WH, Rehak R, Snutch TP, Zamponi GW & Turner RW (2006). Specific T-type calcium channel isoforms are associated with distinct burst phenotypes in deep cerebellar nuclear neurons. *Proc Natl Acad Sci U S A* **103**, 5555–5560.

Mugnaini E, Diño MR & Jaarsma D (1997). The unipolar brush cells of the mammalian cerebellum and cochlear nucleus: cytology and microcircuitry. *Prog Brain Res* **114**, 131–150.

Mugnaini E & Floris A (1994). The unipolar brush cell: a neglected neuron of the mammalian cerebellar cortex. *J Comp Neurol* **339**, 174–180.

Mugnaini E, Floris A & Wright-Goss M (1994). Extraordinary synapses of the unipolar brush cell: an electron microscopic study in the rat cerebellum. *Synapse* **16**, 284–311.

Nagata K, Duggan A, Kumar G & Garcia-Anoveros J (2005). Nociceptor and hair cell transducer properties of TRPA1, a channel for pain and hearing. *J Neurosci* **25**, 4052–4061.

Nilsson P, Hillered L, Olsson Y, Sheardown MJ & Hansen AJ (1993). Regional changes in interstitial $K^+$ and $Ca^{2+}$ levels following cortical compression contusion trauma in rats. *J Cereb Blood Flow Metab* **13**, 183–192.

North RA & Surprenant A (2000). Pharmacology of cloned P2X receptors. *Annu Rev Pharmacol Toxicol* **40**, 563–580.

Nunzi MG, Birnstiel S, Bhattacharyya BJ, Slater NT & Mugnaini E (2001). Unipolar brush cells form a glutamatergic projection system within the mouse cerebellar cortex. *J Comp Neurol* **434**, 329–341.

Parra P, Gulyas AI & Miles R (1998). How many subtypes of inhibitory cells in the hippocampus? *Neuron* **20**, 983–993.

Puopolo M, Bean BP & Raviola E (2005). Spontaneous activity of isolated dopaminergic periglomerular cells of the main olfactory bulb. *J Neurophysiol* **94**, 3618–3627.

Raman IM & Bean BP (1999). Ionic currents underlying spontaneous action potentials in isolated cerebellar Purkinje neurons. *J Neurosci* **19**, 1663–1674.

Raman IM, Gustafson AE & Padgett D (2000). Ionic currents and spontaneous firing in neurons isolated from the cerebellar nuclei. *J Neurosci* **20**, 9004–9016.

Rossi DJ, Alford S, Mugnaini E & Slater NT (1995). Properties of transmission at a giant glutamatergic synapse in cerebellum: the mossy fiber-unipolar brush cell synapse. *J Neurophysiol* **74**, 24–42.

Rudy B & McBain CJ (2001). Kv3 channels: voltage-gated $K^+$ channels designed for high-frequency repetitive firing. *Trends Neurosci* **24**, 517–526.

Sather W, Dieudonne S, MacDonald JF & Ascher P (1992). Activation and desensitization of N-methyl-D-aspartate receptors in nucleated outside-out patches from mouse neurones. *J Physiol* **450**, 643–672.

Sekerková G, Ilijic E, Mugnaini E & Baker JF (2005). Otolith organ or semicircular canal stimulation induces c-fos expression in unipolar brush cells and granule cells of cat and squirrel monkey. *Exp Brain Res* **164**, 286–300.

Simpson JI, Hulscher HC, Sabel-Goedknegt E & Ruigrok TJ (2005). Between in and out: linking morphology and physiology of cerebellar cortical interneurons. *Prog Brain Res* **148**, 329–340.

Taddese A & Bean BP (2002). Subthreshold sodium current from rapidly inactivating sodium channels drives spontaneous firing of tuberomammillary neurons. *Neuron* **33**, 587–600.

Talley EM, Lei Q, Sirois JE & Bayliss DA (2000). TASK-1, a two-pore domain $K^+$ channel, is modulated by multiple neurotransmitters in motoneurons. *Neuron* **25**, 399–410.

Taverna S, Tkatch T, Metz AE & Martina M (2005). Differential expression of TASK channels between horizontal interneurons and pyramidal cells of rat hippocampus. *J Neurosci* **25**, 9162–9170.

von Kugelgen I (2006). Pharmacological profiles of cloned mammalian P2Y-receptor subtypes. *Pharmacol Ther* **110**, 415–432.

## Acknowledgements

We thank Drs Bruce Bean and James Baker for critical reading of the manuscript. This work was supported by N.I.H. grant NS09904 and institutional funds.

## Supplemental material

Online supplemental material for this paper can be accessed at:
http://jp.physoc.org/cgi/content/full/jphysiol.2007.129106/DC1
and
http://www.blackwell-synergy.com/doi/suppl/10.1113/jphysiol.2007.129106